51st AIAA Aerospace Sciences Meeting including the New Horizons Forum and Aerospace Exposition
07 - 10 January 2013, Grapevine (Dallas/Ft. Worth Region), Texas

AIAA 2013-0517

Influence of resolution and Reynolds number on large-eddy simulations of channel flow using relaxation filtering

Francois Kremer*, Christophe Bogey† and Christophe Bailly‡
Laboratoire de Mécanique des Fluides et d'Acoustique
UMR CNRS 5509, Ecole Centrale de Lyon
69134 Ecully Cedex, France

In this work, a large-eddy simulation (LES) approach based on relaxation filtering, validated for free shear flows in a number of previous studies, is applied to turbulent channel flows in order to assess its validity for wall-bounded flows. For this, simulations are performed using different grids, and for various Reynolds numbers. The reliability of the LES results is estimated based on both *a priori* and *a posteriori* analyses. In a first step, a channel flow at a friction Reynolds number Re_τ of 300 is computed using grids with increasing resolution. For mesh spacings equal to and lower than $\Delta x^+ = 30$, $\Delta y^+ = 1$ at the wall and $\Delta z^+ = 10$ in the streamwise, wall-normal and spanwise directions, respectively, the mean and fluctuating velocity profiles appear not to change significantly. For all grids including the coarsest ones, the large near-wall turbulent structures, whose typical size are given by integral length scales and by dominant components in velocity spectra, are found to be well discretized. However, the examination of the transfer functions in the wavenumber space of the dissipation mechanisms, namely molecular viscosity and relaxation filtering, shows that a mesh spacing $\Delta x^+ \leq 30$ is for instance necessary to ensure the physical relevance of the LES solutions, which is in agreement with the findings of the grid-convergence study. In a second step, channel flows at friction Reynolds numbers of 350, 600 and 960 are simulated. The results are very similar to reference data from the literature. Furthermore, the Reynolds number effects in channel flows are well reproduced using the present LES approach.

I. Introduction

Over the last two decades, computational fluid dynamics has become an efficient tool for the study of wall turbulence. In particular, wall-bounded flows at increasing Reynolds number have been simulated, in order to take into account the effects of the Reynolds number on flow statistics and coherent structures, which are subject to important discussions.[1] The dynamics of wall turbulence is strongly influenced by the dynamics of the small scales developing close to the wall, which exhibit strong anisotropy and complex interactions with larger scales. Thus, to properly catch the features of wall-bounded flows, simulations must accurately calculate these small scales. Therefore, most of numerical studies on wall turbulence consist in Direct Numerical Simulation (DNS) of channel flows[2–8] and boundary layers.[9–13] However, as the Reynolds number increases, the computational cost of a DNS becomes rapidly prohibitive. To illustrate this, we can note that twenty years have elapsed between the DNS of channel flows by Kim *et al.*[2] and Hoyas *et al.*,[5] in which the Reynolds numbers differ by one decade only.

In order to reduce the computational cost, Large Eddy Simulations (LES), in which only the larger eddies are resolved, while the effects of the small eddies are modelled, can be used. Classical turbulence models however rely on the assumption that the large scales carry energy, while the small scales have mainly

*PhD, Email: francois.kremer@ec-lyon.fr
†CNRS Research Scientist, Senior AIAA Member
‡Professor at Ecole Centrale de Lyon, Senior AIAA Member

dissipative effects.[14] Since this assumption is not true in the inner part of boundary layers, some LES are performed by resolving the outer part of the wall-bounded flows only, while the inner part is modelled.[15] Very high Reynolds numbers can thus be reached,[16] but the near-wall structures are not reproduced and cannot be studied using this approach. Contrary to wall-modelled LES, wall-resolved LES compute both the outer and inner parts of the flow, at the expense of the computational cost. Accordingly, the range of Reynolds numbers of wall-resolved LES is much smaller, and falls within the range of DNS.[17–20] A significant reduction of the computational cost is however possible. The LES of a boundary layer performed by Schlatter *et al.*,[20] for instance, allowed a reduction of the number of grid points by a factor of 10 with respect to a DNS.

In a wall-resolved LES, various numerical parameters such as the boundary conditions, the grid resolution, the subgrid-scale model and the discretization methods can affect the calculation of near-wall scales. A validation of the simulation method is thus necessary. Such validation should be carried out even for DNS. Schlatter & Örlü[13] has for example reviewed data from several DNS of boundary layers, and pointed out some discrepancies on basic integral quantities and on flow statistics. They showed in particular that flow features are strongly influenced by inflow conditions and turbulence tripping.[21] Such difficulties do not exist in the channel flow case. Indeed, since the turbulence is homogeneous in the streamwise direction, periodic conditions are imposed such that no inflow condition is needed. This flow case can therefore be interesting for the assessment of LES methodology. For example, Rasam *et al.*[22] studied the effect of subgrid-scale model and grid resolution of LES in this way. Similarly, Vuorinen *et al.*[23] performed an LES of a channel flow as a test case for a space discretization method.

In this work, the main objective is to investigate the accuracy of an LES approach for a channel flow case. This approach is based on a relaxation filter which takes into account the dissipative effects of the subgrid scales and leave the larger scales nearly unaffected.[24] It has been previously used in several studies of jet flows[25–29] as well as for a flow around an airfoil[30] or for a turbulent boundary layer.[19] Here, the capacity of LES to properly reproduce the specific mechanisms of wall turbulence is examined by performing a grid convergence study. In particular, our attention will be focused on the near wall region, where the small scales play an important role on the dynamics of the flow. Another objective of the present work is to check the capacity of the LES to reproduce Reynolds number effects. To this end, the effects on the resolved scales of the different dissipation mechanisms, namely the molecular viscosity and the relaxation filter, will be compared. It is indeed mandatory to verify that the dissipation introduced by the subgrid-scale model does not artificially decreases the Reynolds number, as mentioned by Bogey & Bailly.[26–28] The LES can then be used to study Reynolds effects, as made by Bogey & Bailly[29] for jet flows. Here, Reynolds number effects on channel flow are investigated by performing Large-Eddy simulations at three different Reynoldls numbers.

The paper is organized as follows. The validation of the LES method on a channel flow case is presented in section II, including a mesh convergence study, and a discussion about the dissipation mechanisms. A study of the Reynolds number effects on velocity statistics based on the results of several LES is then carried out in section III. Finally, concluding remarks are given in section IV.

II. Influence of grid resolution

II.A. Parameters

A three-dimensional turbulent channel flow at a Reynolds number $Re_\tau = u_\tau h/\nu = 300$ and a Mach number of $M = U_0/c = 0.4$, where U_0 is the centerline velocity, c is the speed of sound, h is the channel half-width, $u_\tau = \sqrt{\tau_w/\rho}$ is the friction velocity, τ_w is the wall shear stress, and ν and ρ are respectively the kinematic viscosity and the density of the flow, is considered. In what follows, the streamwise, wall-normal and spanwise coordinates are denoted by x, y and z, respectively, and the corresponding velocity components are referred to as u, v, and w. The walls are located at $y = 0$ and $y = 2h$. Large-eddy simulations of the channel flow are performed by solving the compressible Navier-Stokes equations on Cartesian meshes. For each of them, the mesh spacings in the streamwise and spanwise directions, namely Δx and Δz, are constant. In the y direction, the mesh spacing is stretched from the wall with an expansion rate r. The mesh space at the wall and at the center of the channel are given by Δy_w and Δy_c, respectively. The sizes of the computational box in the streamwise, wall-normal and spanwise directions are $L_x = 12h$, $L_y = 2h$ and $L_z = 6h$. The spatial derivatives are computed using an explicit 4th-order 11-point finite-difference scheme.[31] Periodic boundary conditions are implemented in the x and z directions. In the y direction, a no-slip condition is imposed at the wall. Time integration is performed with an explicit fourth-order six-step Runge Kutta scheme.[32] An explicit 6th-order 11-point selective filter[24] is used for the relaxation filtering,

and remove spurious grid-to-grid oscillations.

II.B. Grid convergence of velocity profiles

A grid-convergence study is carried out by performing simulations on fourteen Cartesian grids, characterized by the mesh spacing given in table 1 in wall units. The mesh convergence is investigated in the y direction using different grids in which the mesh spacing at the wall in the y direction decreases from $\Delta y_w^+ = 3.5$ down to 0.47, while it is set constant at the center of the channel, with $\Delta y_c^+ = 15$. In the other directions, the mesh spacing are set to $\Delta x^+ = 15$ and $\Delta z^+ = 7.5$. For the mesh-convergence study in the z direction, the value of Δz^+ decreases from 15 down to 5, and $\Delta x^+ = 15$, $\Delta y_w^+ = 0.95$ and $\Delta y_c^+ = 15$ are fixed. Finally, for the mesh-convergence study in the x direction, the mesh spacing decreases from $\Delta x^+ = 45$ down to 15, and $\Delta z^+ = 7.5$, $\Delta y_w^+ = 0.95$ and $\Delta y_c^+ = 15$ in all cases. The mesh spacings in the LES of a channel flow performed by Viazzo *et al.*,[17] and in the LES of boundary layers carried out by Gloerfelt & Berland[19] and by Schlatter *et al.*[20] are also given in table 1 for the comparison. Since the dimensions of the domain are constant, the number of mesh points in the different grids varies, yielding $87 \leq n_x \leq 257$, $85 \leq n_y \leq 161$ and $129 \leq n_z \leq 385$. For each grid, a time step Δt is chosen such that $\mathrm{CFL}_y = c\Delta t/\Delta y_w \approx 0.8$, ensuring the stability of time integration.

Table 1. Parameters of the grids used for the mesh convergence study, and for LES from the literature[17, 19, 20] ; the mesh spacings are normalized by the viscous length scale, Δx^+ and Δz^+ : mesh spacings in the x and z directions, Δy_w^+ and Δy_c^+ : mesh spacings in the y direction at the wall and at the center of the channel, r : expansion rate of the mesh spacing in the y direction.

Grids	Δx^+	Δz^+	Δy_c^+	Δy_w^+	r (%)
Ygrid1	15	7.5	15	**3.7**	3.5
Ygrid2	15	7.5	15	**1.9**	4.0
Ygrid3	15	7.5	15	**0.95**	4.4
Ygrid4	15	7.5	15	**0.47**	4.5
Zgrid1	15	**15**	15	0.95	4.4
Zgrid2	15	**12.5**	15	0.95	4.4
Zgrid3	15	**10**	15	0.95	4.4
Zgrid4	15	**7.5**	15	0.95	4.4
Zgrid5	15	**5**	15	0.95	4.4
Xgrid1	**45**	7.5	15	0.95	4.4
Xgrid2	**35**	7.5	15	0.95	4.4
Xgrid3	**30**	7.5	15	0.95	4.4
Xgrid4	**25**	7.5	15	0.95	4.4
Xgrid5	**15**	7.5	15	0.95	4.4
Viazzo *et al.*[17]	31.4	15.7	51.84	0.88	
Gloerfelt & Berland[19]	37	14.7		0.98	2
Schlatter *et al.*[20]	25.3	10.8	14.2	<1	

The mesh convergence is discussed by examining the profiles of mean streamwise velocity $U^+ = U/u_\tau$ and of rms streamwise velocity $u_{rms}^+ = \sqrt{\overline{u'^2}}$, represented as a function of the wall distance $y^+ = yu_\tau/\nu$. The results of the mesh convergence in the y direction are shown in figure 1. In figure 1(a), the mean velocity profiles obtained with $\Delta y_w^+ = 3.7$, 1.9 and 0.95 differ, whereas those obtained with $\Delta y_w^+ = 0.95$ and 0.47 are very close. Similar observations can be made for the rms velocity profiles in figure 1(b), where results are converged with respect to the grid for $\Delta y_w^+ = 0.95$. It can be noted that the simulations carried out with the two coarsest grids underestimated values of U^+ and u_{rms}^+. The peak of the rms velocity profile in figure 1(b) is in particular very sensitive to the value of Δy_w^+, highlighting the importance of the first grid point in the y direction.

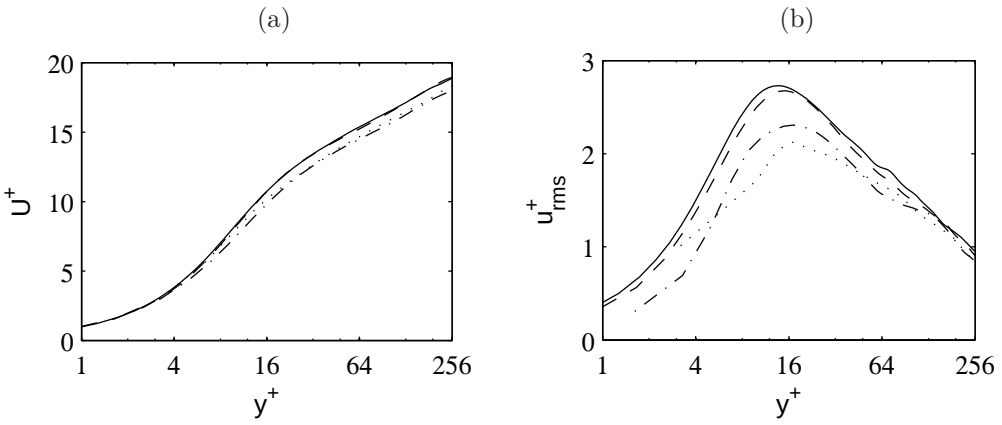

Figure 1. Representation of (a) mean, and (b) rms streamwise velocities as a function of the wall distance, for ····· $\Delta y_w^+ = 3.7$, — · — · — $\Delta y_w^+ = 1.9$, — — — $\Delta y_w^+ = 0.95$, ——— $\Delta y_w^+ = 0.47$.

The mean and rms velocity profiles obtained in the simulations performed with the grids where Δz^+ varies between 5 and 15 are represented in the figure 2. The fluctuating velocity profiles are very close for $\Delta z^+ = 5$, 7.5 and 10, as it can be seen in the figure 2(b). Concerning the mean velocity profiles in figure 2(a), small discrepancies are noticed in the outer part of the flow, but the agreement is good for $y^+ < 100$. The convergence is thus practically reached for $\Delta z^+ = 10$.

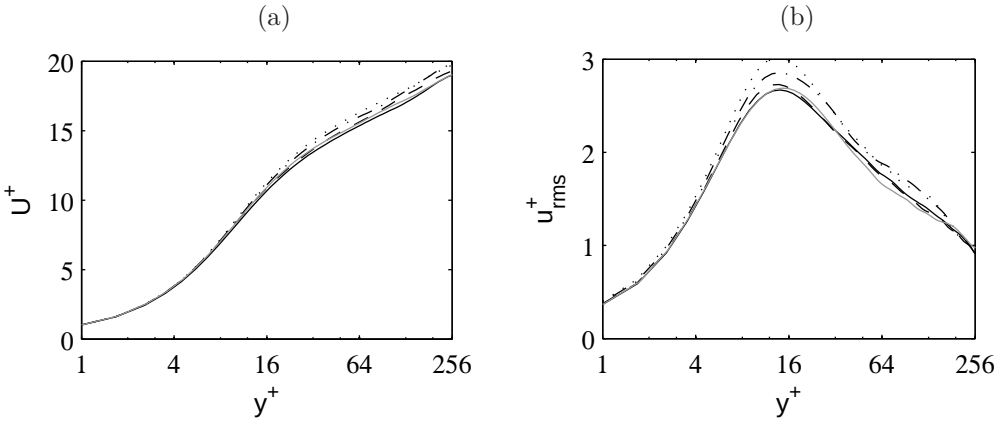

Figure 2. Representation of (a) mean, and (b) rms streamwise velocities as a function of the wall distance, for ····· $\Delta z^+ = 15$, — · — · — $\Delta z^+ = 12.5$, — — — $\Delta z^+ = 10$, ——— $\Delta z^+ = 7.5$, ——— $\Delta z^+ = 5$.

Finally, the results obtained with the LES carried out on grids with $15 \leq \Delta x^+ \leq 45$ are presented in figure 3. The mean velocity profiles in figure 3(a) differ for $\Delta x^+ = 30$, 35 and 45, but are similar for $\Delta x^+ = 15$, 25 and 30. Similar remarks can be made for the fluctuating velocity in figure 3(b), whose profiles are close for $\Delta x^+ = 15$, 25 and 30. Therefore, the convergence is obtained for $\Delta x^+ = 30$.

II.C. Effects on turbulence properties

As mentioned in the introduction, the LES of a wall-bounded flow must accurately compute the turbulent structures developping close to the wall. This is verified here for the grids used in the mesh-convergence study. More precisel, we focus our attention on the buffer layer, by calculating some characteristic length scales at a distance $y^+ = 16$ corresponding roughly to the location of the peak of the rms streamwise velocity. By comparing these length scales to the mesh spacings Δx and Δz, the quality of discretization of the turbulent structures can be estimated.

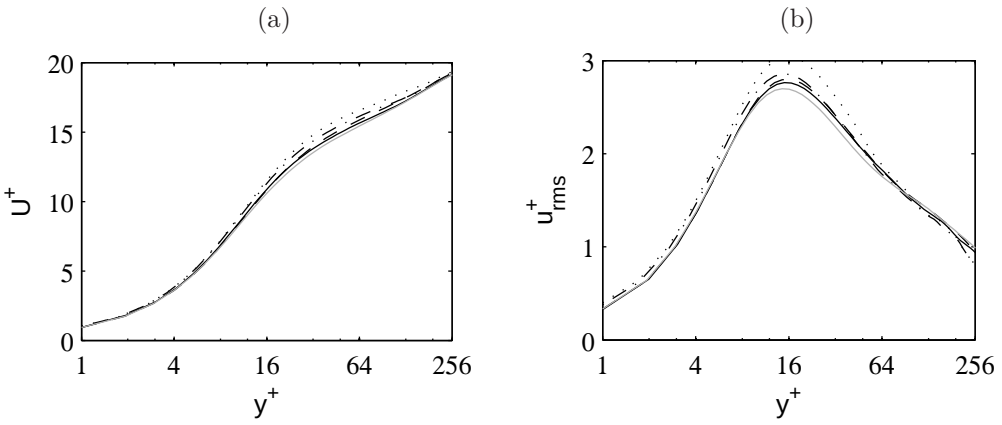

Figure 3. Representation of (a) mean, and (b) rms streamwise velocities as a function of the wall distance, for ------- $\Delta x^+ = 45$, — · — · — $\Delta x^+ = 35$, — — — $\Delta x^+ = 30$, ——— $\Delta x^+ = 25$, ——— $\Delta x^+ = 15$.

II.C.1. Integral length scales

A first estimation of the size of the turbulent structures, integral length scales, are calculated from the results obtained with one of the grid-converged LES presented above, namely the simulation carried out using $\Delta x^+ = 15$, $\Delta z^+ = 5$ and $\Delta y_w^+ = 0.95$. The integral length scales in the streamwise and spanwise directions are given respectively by :

$$\left\{ \begin{array}{l} L_{uu}^{(x)} = \displaystyle\int_0^\infty \mathcal{R}_{uu}(x,0)dx \\ L_{uu}^{(z)} = \displaystyle\int_0^\infty \mathcal{R}_{uu}(0,z)dz \end{array} \right. \tag{1}$$

where

$$\mathcal{R}_{uu}(x,z) = \frac{\overline{u'(x_0,y_0,z_0)u'(x_0+x,y_0,z_0+z)}}{\overline{u'^2(y_0)}} \tag{2}$$

is the correlation coefficient of the streamwise velocity taken at the wall distance $y_0^+ = 16$. The overbar denotes averaging over time and over all the positions (x_0, z_0) because turbulence is homogeneous in the x and z directions. The variations of $\mathcal{R}_{uu}(x,0)$ and $\mathcal{R}_{uu}(0,z)$ are represented in the figure 4 as a function of separation distances normalized by wall units. As expected, in the two directions, the correlations coefficients tends to 0 as the separation distance increases. Furthermore, $\mathcal{R}_{uu}(0,z)$ is seen to decrease faster than $\mathcal{R}_{uu}(x,0)$, and presents a negative hump between $z^+ = 40$ and 200. By integrating these curves, we obtain integral length scales $L_{uu}^{(x)^+} = 210$ and $L_{uu}^{(z)^+} = 20$. Note that for practical reasons, the integration of $\mathcal{R}_{uu}(0,z)$ is performed up to $z_{max}^+ = 40$ such that $\mathcal{R}_{uu}(0,z_{max}) = 0$, to avoid an artificial reduction of the value of $L_{uu}^{(z)}$. For the calculation of $L_{uu}^{(x)}$, the coefficient $\mathcal{R}_{uu}(x,0)$ is integrated up to $x = L_x/2$.

The quality of the discretization of turbulent structures is estimated from the ratios of the integral length scales with respect to the corresponding mesh spacings. These ratios are reported in table 2 for different values of Δx^+ and Δz^+. In the streamwise direction, the length scale $L_{uu}^{(x)}$ is discretized by more than 4.6 points for all values of Δx^+. On the contrary, in the spanwise direction, the integral length scale $L_{uu}^{(z)}$ is discretized by less than 4 points for every value of Δz^+. The discretization becomes even lower than 2 points per integral length scale for $\Delta z^+ > 10$. Considering that wavelengths shorter than about 4 points per wavelength are damped by the relaxation filter, it seems that for all the simulations presented in section II.B, the turbulent structures in the buffer layer are well resolved in the streamwise direction, but might be under resolved in the spanwise direction. However, the integral length scale is a rough measure of the size of the turbulent structures, and a further analysis is necessary.

II.C.2. Spanwise velocity spectra

A more reliable estimation of the size of the turbulent structures can be obtained from the power spectral density of velocity fluctuations. The spanwise spectra $\phi_{uu}(k_z)$ of the streamwise velocity fluctuations are

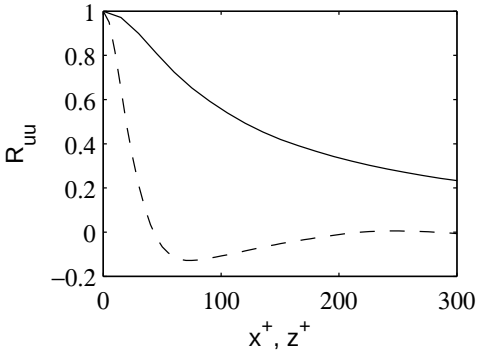

Figure 4. Correlation coefficients obtained for the streamwise velocity at $y^+ = 16$ from the simulation performed with $\Delta x^+ = 15$ and $\Delta z^+ = 5$, in the directions x and z : ——— $R_{uu}(x,0)$, – – – $R_{uu}(0,z)$.

Table 2. Ratios between the integral length scales $L_{uu}^{(x)}$ and $L_{uu}^{(z)}$ and the corresponding mesh spacings for different values of Δx^+ and Δz^+ ($L_{uu}^{(x)}$ and $L_{uu}^{(x)}$ calculated from the results obtained with the finest grid).

Δx^+	$L_x/\Delta x$	Δz^+	$L_z/\Delta z$
45	4.6	15	1.4
35	6.0	12.5	1.6
30	7.0	10	2.0
25	8.4	7.5	2.7
15	14	5	4.0

computed from the data of the three LES Zgrid1, Zgrid3 and Zgrid4 performed with an identical value of $\Delta x^+ = 15$, but different values of $\Delta z^+ = 15$, 10 and 7.5. They are represented in figure 5 as a function of the spanwise wavenumber k_z, normalized by wall units. The axes are in logarithmic scales. The spectra look similar. They slightly increase with wavenumeber in the low-wavenumber region, reach a maximum around $k_z^{max+} = 0.038$, indicated by a vertical grey line, and then decrease. In the high wavenumber region, the different spectra exhibit a sudden collapse at wavenumbers $k_z^+ = 0.07$, 0.1 and 0.15 for the simulations performed with $\Delta z^+ = 15$, 10 and 7.5, respectively. In all cases, the corresponding wavelengths $\lambda_z = 2\pi/k_z$ are discretized by approximately $\lambda_z/\Delta z = 6$ points. The observed sharp decreases are thus due to the relaxation filtering, which damps wavelengths shorter than about $4\Delta z$.

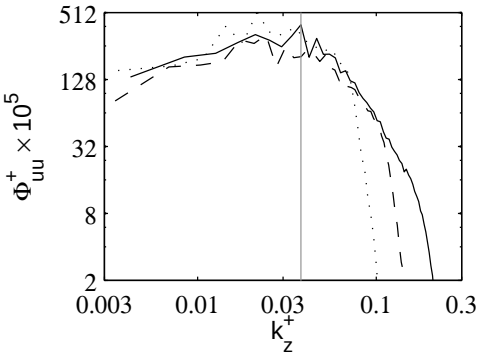

Figure 5. Power spectral densities of the streamwise velocity fluctuations ϕ_{uu}^+ obtained at $y^+ = 16$ in the simulations using ····· $\Delta z^+ = 15$, – – – $\Delta z^+ = 10$, and ——— $\Delta z^+ = 7.5$, as a function of the spanwise wavenumber k_z^+. The vertical gray line indicates the wavelength $\lambda_z^{max+} = 166$, corresponding to the most energetic scales.

Although high-wavenumber components are significantly affected by the spectral truncation, the most energetic scales are found at $\lambda_z^{max+} = 2\pi/k_z^{max+} = 166$ in all cases. The ratio between this wavelength and the spanwise mesh spacing is calculated and given in table 3 for different values of Δz^+. It varies from 11 for $\Delta z^+ = 15$ up to 33 for $\Delta z^+ = 5$. Therefore, even with the coarsest grid, the most energetic spanwise structures are well discretized.

Table 3. Ratios between the wavelength λ_z^{max} of the most energetic spanwise structures and the spanwise mesh spacing for different values of Δz^+.

Δz^+	$\lambda_z^{max}/\Delta z$
15	11
12.5	13
10	16
7.5	22
5	33

II.D. Dissipation transfer functions

In the present LES approach, dissipation is provided by the molecular viscosity, as well as by the relaxation filter. If the latter induces more dissipation than the former at larger scales, the effective Reynolds number of the simulation might be lower than the expected value. The magnitude of the two dissipation mechanisms can be compared in the wavenumber space, as proposed by Bogey *et al.*[28] The transfer function associated with molecular viscosity is given by $\nu(k\Delta)^2/\Delta^2$, where $k\Delta$ is the normalized wavenumber, and Δ is an arbitrary mesh spacing. The transfer function associated with relaxation filtering is then $\sigma D^*(k\Delta)/\Delta t$, where $D^*(k\Delta)$ is the damping factor of the filter, and σ is the filtering strength.

The transfer functions are calculated here for the simulations performed in section II.B with the grids where $\Delta z^+ = 7.5$ and $\Delta y_w = 0.95$ are fixed, and Δx^+ varies between 15 and 45. The time step used in the simulations is defined by $\Delta t = 0.8\Delta y_w/c$. Concerning the relaxation filter, the 11-points 6th-order explicit filter of Bogey[24] is applied every time iteration with a strength $\sigma = 1$. The transfer functions obtained for these parameters are represented in figure 6 as a function of the normalized wavenumber $k\Delta$, using axes in logarithmic scales. Since the transfer function associated with molecular viscosity depends on the mesh spacing, four curves are noted for $\Delta^+ = 7.5$, 15, 30 and 45. The first curve provides the dissipation in the spanwise direction, where $\Delta z^+ = 7.5$, while the other three curves provide the dissipation in the streamwise direction for the three different value of the mesh spacing $\Delta x^+ = 15$, 30 and 45.

For $\Delta^+ = 7.5$, the dissipation transfer function associated with molecular viscosity is higher than that associated with relaxation filtering for $k\Delta < 1.1$, and lower for $k\Delta > 1.1$. This means that wavelengths discretized by more than $\lambda/\Delta = 2\pi/1.1 = 5.7$ points are mainly dissipated by molecular viscosity, while shorter wavelengths are damped by the relaxation filtering. A similar behavior is noticed for $\Delta^+ = 15$, where the two transfer functions intersect at $k\Delta = 1.0$, corresponding to wavelength discretized by $\lambda/\Delta = 6.3$ points. Thus, in the LES using $\Delta x^+ = 15$ and $\Delta z^+ = 7.5$, the dynamics of most of the turbulent scales is driven by viscous dissipation, while the filter affects only the structures with relatively small extent in the streamwise and spanwise directions.

For $\Delta^+ = 30$, the dissipation by molecular viscosity is now more stronger than the filtering dissipation for $k\Delta < 0.48$. For higher wavenumbers, they are of the same order of magnitude, and finally the filtering dissipation becomes dominant for $k\Delta > 0.95$. This means that in the LES performed with $\Delta x^+ = 30$, the filtering significantly affects the structures whose streamwise extent is up to $\lambda/\Delta x = 2\pi/0.48 = 13$ mesh points. Similarly, for $\Delta^+ = 45$, the viscous dissipation level is higher than the filtering dissipation for $k\Delta < 0.35$, and lower for $k\Delta > 0.35$. The streamwise extent of the structures affected by the filter is in this case up to $\lambda/\Delta x = 18$ mesh points. Hence, in the two LES performed with $\Delta x^+ = 30$ and 45, the relaxation filter damps an important part of the turbulent scales.

These results show that, using highly selective filter and a sufficiently fine grid, the dynamics of the resolved scale is governed by physical mechanism associated with molecular viscosity, and not by artifical damping due to the filtering. This might be not the case for the LES performed with $\Delta x^+ = 30$ and 45, where the streamwise mesh spacing are too coarse. Therefore, the effective Reynolds number is likely not to be decreased only in the former cases.

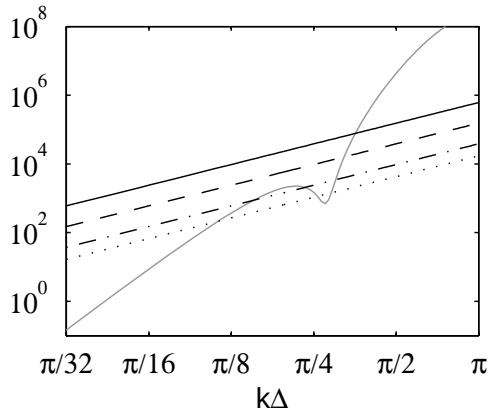

Figure 6. Representation of the dissipation transfer functions associated with ——— relaxation filtering, and with molecular viscosity for ····· $\Delta^+ = 45$, – · – · – $\Delta^+ = 30$, – – – $\Delta^+ = 15$ and ——— $\Delta^+ = 7.5$, according to the normalized wave number $k\Delta$.

III. Effects of the Reynolds number

III.A. Parameters

In order to investigate the effects of the Reynolds number, large-eddy simulations of turbulent channel flows at Reynolds numbers $Re_\tau = 350$, 600 and 960, referred to as Re350, Re600 and Re960, are performed. The Mach number is fixed at 0.5 for the three cases. The parameters of the grids used in the different simulations are given in table 4. The Re350 simulation is carried out with mesh spacing $\Delta x^+ = 17$, $\Delta z^+ = 8.5$, and $\Delta y_w^+ = 0.97$ at the wall and $\Delta y_c^+ = 16$ at the center of the channel in the wall-normal direction. The grids used in the Re600 and Re960 cases are slightly coarser in the homogeneous directions, where $\Delta x^+ = 25$ and $\Delta z^+ = 10$ are set. In the wall normal direction, the mesh spacing at the wall is $\Delta y_w^+ = 0.97$ for Re600, and $\Delta y_w^+ = 0.93$ for Re960. At the center of the channel, the mesh spacing is $\Delta y_c^+ = 10$ in both cases. These values of mesh spacings are smaller than, or at least equal to the minimal values required according to the mesh-convergence study conducted in section II. The number of mesh points is reported in table 4. It varies from 8.1 millions for Re350 to 68 millions for Re960.

Table 4. Parameters for the LES of a channel flow ; Re_τ : Reynolds number, M : Mach number, $n = n_x \times n_y \times n_z$: number of grid points, Δx^+, Δz^+, Δy_w^+ et Δy_c^+ : mesh spacings.

Case	Re_τ	M	$n_x \times n_y \times n_z$	n	Δx^+	Δz^+	Δy_w^+	Δy_c^+
Re350	350	0.5	$247 \times 133 \times 247$	8.1×10^6	17	8.5	0.97	16
Re600	600	0.5	$285 \times 185 \times 355$	19×10^6	25	10	0.97	10
Re960	960	0.5	$457 \times 261 \times 571$	68×10^6	25	10	0.93	10

Time integration parameters are collected in the table 5. The time integration of the Re350 simulation is performed using a fourth-order six-step explicit Runge Kutta scheme.[32] The CFL number at the wall in the wall normal direction $\mathrm{CFL}_y = c\Delta t/\Delta y_w$, where Δt is the time step, is 0.8. For the Re600 and Re960 cases, in order to reduce the computational time, a third-order six-step semi-implicit Runge Kutta scheme is used. A detailled description of this scheme can be found in a previous paper.[33] The CFL number in the spanwise direction $\mathrm{CFL}_z = c\Delta t/\Delta z$ is equal to 1.0, yielding a CFL number at the wall of $\mathrm{CFL}_y = 11$. The physical duration of the simulations is $T_{tot}U_0/h = 490$, 203 and 165, and the number of time iterations is $n_{it} = 480000$, 24000 and 35000 for the Re350, Re600 and Re960 computations, respectively.

The numerical methods used for spatial discretization and filtering are the same as those described in section II. Spatial derivatives are approximated using a 4th-order 11-point finite-difference scheme.[31] The effects of the subgrid scales are taken into account by applying a relaxation filtering at every iteration. A 6th-order 11-point explicit selective filter[24] is implemented with a filtering strengh $\sigma = 0.99$.

Table 5. Time integration parameters for the LES of a channel flow ; $\mathbf{CFL}_z = c\Delta t/\Delta z$: CFL number in the spanwise direction, $\mathbf{CFL}_y = c\Delta t/\Delta y_w$: CFL number in the wall normal direction at the wall, Δt : time step, in seconds, $T_{tot}U_0/h$: physical duration of the simulations, scaled by the centerline velocity U_0 and the half width of the channel h, n_{it} : number of time iterations.

Case	algorithm	CFL_z	CFL_y	Δt (s)	$T_{tot}U_0/h$	n_{it}
Re350	explicit RK[32]	0.1	0.8	4.4×10^{-9}	490	480000
Re600	semi-implicit RK[33]	1.0	11	5.6×10^{-8}	203	24000
Re960	semi-implicit RK[33]	1.0	11	5.8×10^{-8}	165	35000

III.B. Dissipation transfer functions

Since the aim of the present study is to investigate the possibility of studying Reynolds number effects with an LES, strength of the dissipative mechanisms governing the dynamics of the flow must be evaluated in the same way as in section II.D, in order to ensure that the effective Reynolds number is not diminished artificially. The dissipation transfer functions associated with molecular viscosity and with relaxation filtering are thus computed for each simulation. The transfer functions are here computed in the streamwise direction, yielding $\nu(k_x\Delta x)^2/\Delta x^2$ for viscous dissipation, and $\sigma D^*(k_x\Delta x)/\Delta t$ for filtering dissipation. The transfer functions obtained in the Re350 case are given in figure 6(a). It can be seen that the two curves intersect at $k_x\Delta x = 1.0$. Viscous dissipation is consequently more important than filtering dissipation for components discretized by more than $\lambda_x/\Delta x = 2\pi/1.0 = 6.3$ points per wavelength, while shorter components are mainly damped by the relaxation filtering. Similarly, for the Re600 and Re960 case in figures in figure 6(b) and 6(c), the viscous dissipation is dominant for components discretized by more than $\lambda_x/\Delta x = 5.7$ points per wavelength. These results show that in the simulations, molecular viscosity provides dissipation of most of the resolved scales. Therefore, the LES are expected to reproduce Reynolds number effects in the present work.

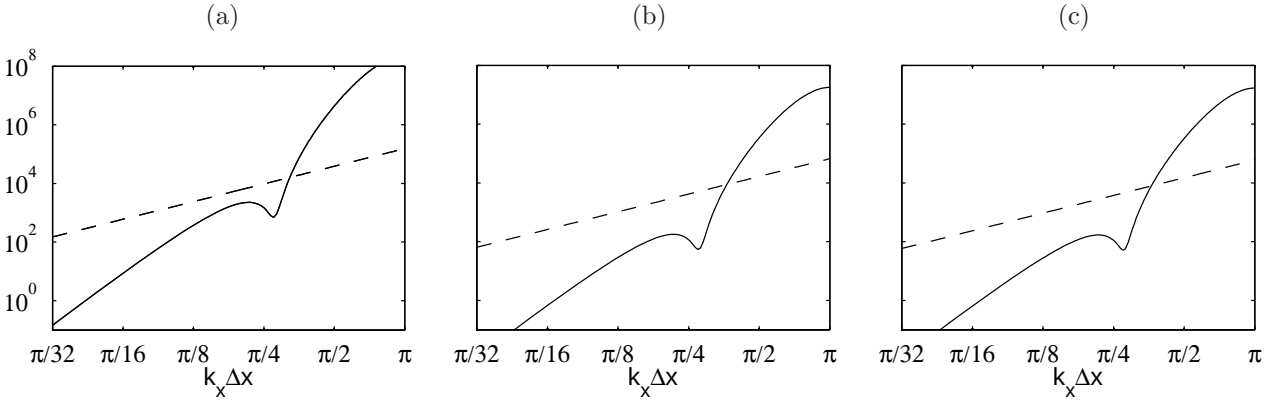

Figure 7. Representation of the dissipation transfer functions associated with ——— relaxation filtering, and with – – – molecular viscosity, according to the streamwise normalized wave number $k_x\Delta x$ for the simulations (a) Re350, (b) Re600 and (c) Re960.

III.C. Flow visualization

To illustrate the fine resolution of the near-wall structures in the present LES, snapshots of the velocity fields obtained at a distance to the wall of $y^+ = 18$ are presented in figure 8 for the Re600 and Re960 cases. Figures 8(a-b) show fields of the streamwise velocity, in which the low-speed regions are in black, and the high-speed regions are in grey. No significant difference is observed between the Re600 case in figure 8(a) and the Re960 case in figure 8(b). Both exhibit high-speed and low-speed regions elongated in the streamwise direction, which correspond to the well-known high- and low-speed near-wall streaks.[34]

Snapshots of wall-normal velocity are displayed in figures 8(c) and 8(d) for the Re600 and Re960 cases, respectively. In these figures, black regions correspond to fluid moving toward the wall, and grey regions correspond to fluid moving away from the wall. The velocity field exhibit a great number of structures consisting in pairs of black and gray regions elongated in the streamwise direction, which are induced by

quasi-streamwise vortices.[34]

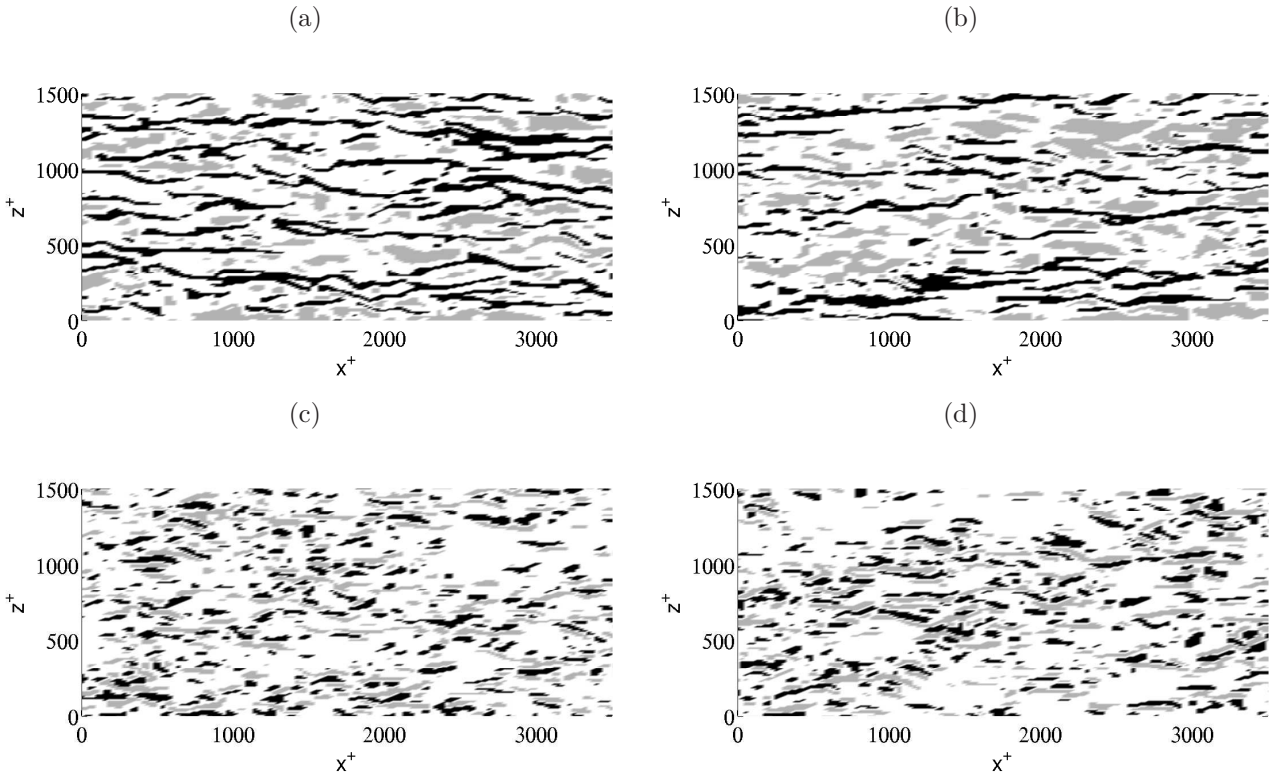

Figure 8. Velocity snapshots in a wall-parallel plane at $y^+ = 18$ for (a,c) Re600 and (b,d) Re960; (a,b) streamwise velocity u; black zones : $u < U - u_{rms}$, white zones : $U - u_{rms} < u < U + u_{rms}$, grey zones : $u > U + u_{rms}$; (c,d) wall-normal velocity v; black zones : $v < -v_{rms}$, white zones : $-v_{rms} < v < v_{rms}$, grey zones : $v > v_{rms}$; snapshots of u and v velocities are taken at the same time on the same part of the domain.

III.D. Mean and fluctuating velocities

The profiles of the mean streamwise velocity $U^+ = U/u_\tau$ obtained from the Re350, Re600 and Re960 simulations are presented in figure 9 as a function of the distance to the wall $y^+ = yu_\tau/\nu$ given in logarithmic scale. The profiles are superimposed for $y^+ < 100$, where they follow similarity laws $U^+ = f(y^+)$, represented by dots in the figure. The law is linear in the viscous sublayer, for $y^+ \leq 5$, and logarithmic for $30 < y^+ < 100$, where the mean velocity profiles follow $U^+ = \ln(y^+)/\kappa + B$ with $\kappa = 0.41$ and $B = 5$. These values of κ and B fall within the range of values observed in numerical and experimental data.[36] For $y^+ \geq 100$, the profiles visibly differ, which is expected because the velocity scales with outer variables in this case.[35]

The fluctutating streamwise velocity $u^+_{rms} = u_{rms}/u_\tau$ is represented as a function of the distance to the wall y^+, given in logarithmic scale, in figure 10(a) for the Re350, Re600 and Re960 cases. The obtained profiles are very similar in the buffer region defined by $5 \leq y^+ \leq 50$. The peak of rms velocity is located at $y^+ \approx 14.5$, and slightly increases with the Reynolds number as observed, for example, in the DNS by Hu *et al.*[7] of channel flows at $Re_\tau = 90 - 1440$. Another change with the Reynolds number can be noted for $y^+ \geq 50$, where the u^+_{rms} profiles present a hump which grows in magnitude and shifts toward higher values of y^+ when the Reynolds number increases. In 10(b), the rms velocity profiles are represented as a function of y/h. In this case, they are not superimposed in the buffer layer, whereas they almost collapse in the outer layer for $y/h > 0.2$. The fluctuating streamwise velocity thus seems to follow a similarity law in the outer region when a mixed scaling is used, namely u_τ for the velocity scale and h for the length scale.

III.E. Comparison with DNS

The mean and fluctuating velocity profiles are compared with reference data from the literature. These data are provided by the DNS of channel flows at $Re_\tau = 395$ and 590 of Moser *et al.*,[8] and at $Re_\tau = 950$ of del Alamo & Jiménez.[3] The mean velocity profiles obtained in the Re350 simulation and the DNS at $Re_\tau = 395$,

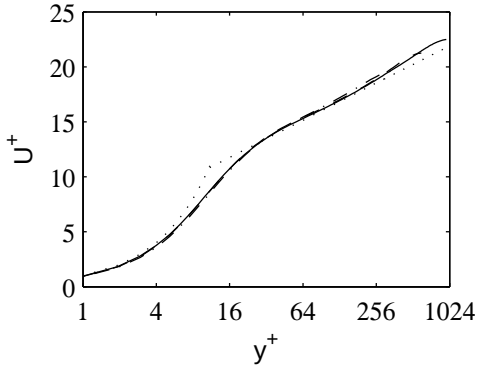

Figure 9. Representation of mean streamwise velocity U^+ as a function of y^+, obtained from Re350, Re600, and Re960; the dots represent the similarity laws $U^+ = y^+$ for $y^+ \leq 10$, and $U^+ = \ln(y^+)/\kappa + B$ with $\kappa = 0.41$ and $B = 5$ for $y^+ \geq 10$.

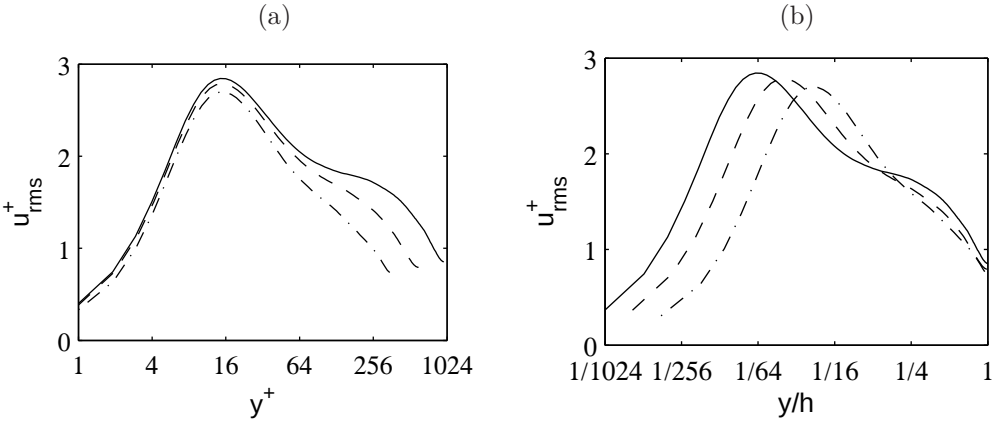

Figure 10. Representation of rms streamwise velocity u^+_{rms} obtained from Re350, Re600 and Re960, as a function of distances (a) y^+ and (b) y/h.

presented in figure 11(a), almost collapse. The streamwise, wall-normal and spanwise fluctuating velocity profiles are shown in figure 11(b). Again, the LES and DNS results are very close, although the fluctuation levels from DNS are slightly higher than those from LES. This might be due to the small difference between the Reynolds numbers of the two simulations.

The mean and fluctuating velocity profiles obtained from the Re600 simulation and the DNS at $Re_\tau = 590$ of Moser *et al.*[8] are represented in figure 12. The agreement between the two simulations is excellent for the mean velocity in figure 12(a), as well as for the fluctuating velocities in figure 12(b). In particular, the hump of the streamwise velocity fluctuations around $y^+ = 200$, which was pointed out based on the LES results in the section III.D, also exists in the DNS results.

Finally, the mean and fluctuating velocity profiles obtained from the Re960 simulation and the DNS at $Re_\tau = 960$ of del Alamo & Jiménez[3] are given in figure 13. Again, the LES and DNS results are in very good agreement for the mean velocity on figure 12(a), as well as for the fluctuating velocities on figure 12(b).

These comparisons with DNS demonstrate that the present LES are reliable and take into account Reynolds number effects both qualitatively and quantitatively.

III.F. Velocity spectra

Finally, power spectral densities ϕ_{uu} of the streamwise velocity are computed in the buffer region, at a distance to the wall $y^+ = 18$, for the Re350, Re600 and Re960 cases. They are represented as a function of the spanwise wavenumber k_z using normalisation by inner scales in figure 14(a). The axes are in logarithmic scales. In the low wavenumber region, for $k_z^+ < 0.02$, strong differencies are observed between the levels obtained in the different cases. This part of the spectra will be described later. For $k_z^+ \geq 0.02$, the spectra

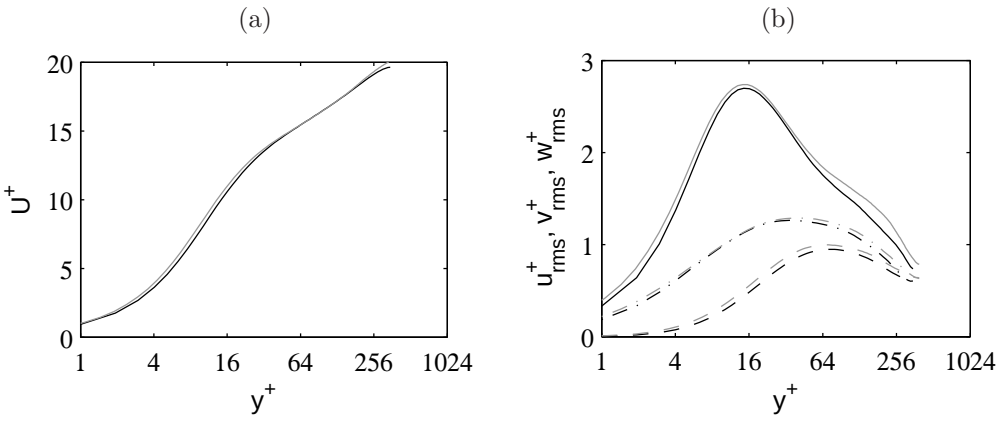

Figure 11. Velocity profiles obtained from Re350 and from the DNS of Moser *et al.*[8] at $Re_\tau = 395$: (a) mean streamwise velocity U^+ and (b) fluctuating velocities u^+_{rms}, v^+_{rms}, w^+_{rms}.

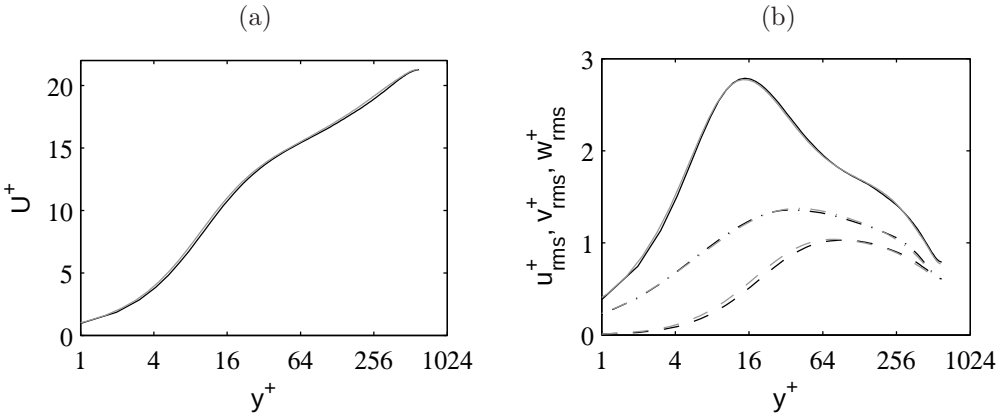

Figure 12. Velocity profiles obtained from Re600 and from the DNS of Moser *et al.*[8] at $Re_\tau = 590$: (a) mean streamwise velocity U^+ and (b) fluctuating velocities u^+_{rms}, v^+_{rms}, w^+_{rms}.

from Re600 and Re960 are superimposed, and that of Re350 is very close to the latters. The three spectra are rather flat between $k_z^+ = 0.02$ and 0.035, and then slightly decrease. Their slope is constant between $k_z^+ = 0.06$ and 0.15, and becomes steeper for $k_z^+ \geq 0.15$. The steeper slope is due to the relaxation filtering. Indeed, given that the filtering damps the wavelengths shorter than $4\Delta z$, the cutoff wavenumber is $k_z^+ = 0.19$ for Re350 and 0.15 for Re600 and Re960.

The use of an inner normalization thus allows to superimpose the velocity spectra obtained at different Reynolds number for wavenumbers $k_z^+ \geq 0.02$. This illustrates the independance of the small structures located in the buffer region, namely the near-wall streaks, from the outer scales of the flow. Furthermore, in figure 14(a), the spanwise scales of the most energetic components, regardless the region $k_z^+ < 0.02$, are located at $k_z^+ = 0.02 - 0.035$. Hence, the most energetic streaks have a spanwise scale in the range $\lambda_z^+ = 180$ and 300, which is higher than the classical spanwise separation of 100 wall units found in the literature.[37] Tomkins & Adrian[38] obtained experimentally a similar shift in a turbulent boundary layer at $Re_\tau = 426$, in which they measured dominant energetic spanwise scales between $\lambda_z^+ = 200$ and 400.

We now consider the low wavenumber region with $k_z^+ \leq 0.02$ in figure 14(a). In the spectrum obtained from Re960, dominant components are found for $k_z^+ = 0.003 - 0.005$. Dominant components are also found in the spectrum of the Re600 case for $k_z^+ = 0.005 - 0.01$, but their magnitude is two times smaller than that obtained from Re960. Finally, in the Re360 case, the spectral levels are two times smaller than those of Re600, and exhibits no significant peak. The increase of the Reynolds number thus results in the growth of the magnitude of low-wavenumber components. These amplified components seem not to scale using wall units. On the contrary, when scaled using outer units as shown on figure 14(b), the spectra are in good agreement for spanwise wavenumbers in the range $3 \leq k_z h \leq 6$, corresponding to spanwise wavelengths

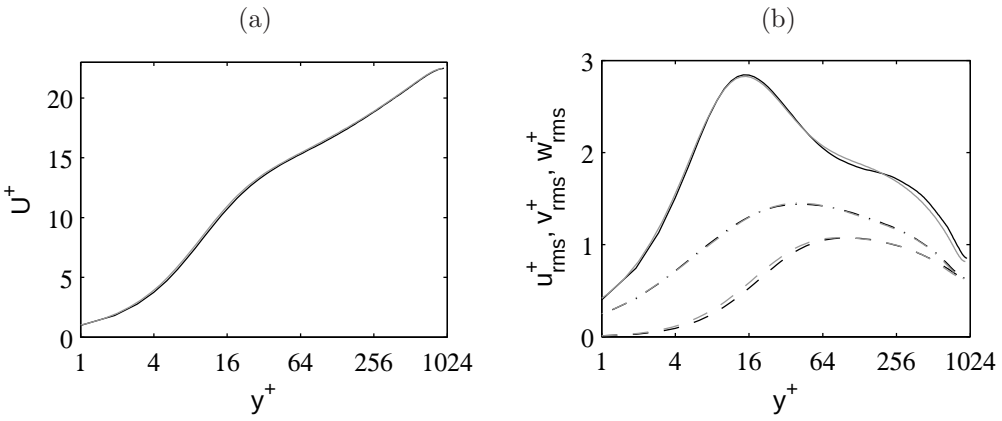

Figure 13. Velocity profiles obtained from Re960 and from the DNS of del Alamo & Jiménez[3] at $Re_\tau = 950$: (a) mean streamwise velocity U^+ and (b) fluctuating velocities u^+_{rms}, v^+_{rms}, w^+_{rms}.

between $1 \leq \lambda_z/h \leq 2$. The low-wavenumber components are thus related to the outer scales of the flow.

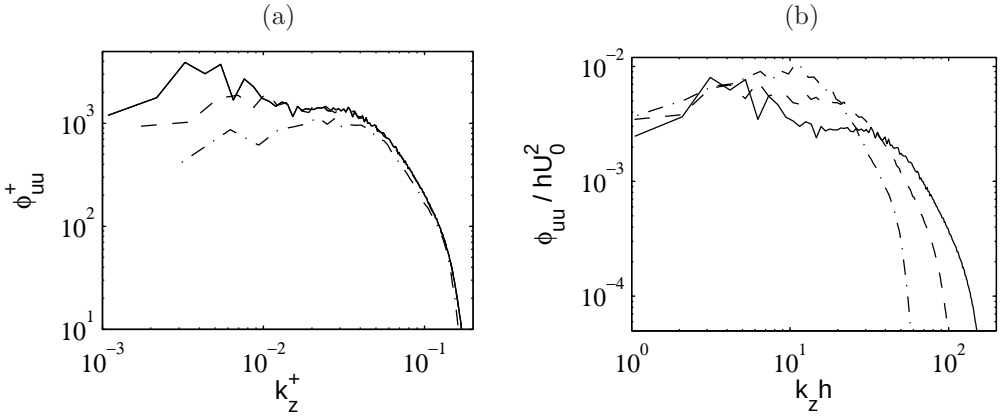

Figure 14. Power spectral densities of the streamwise velocity as a function of the spanwise wavenumber k_z, with (a) inner scaling, and (b) outer scaling, computed at $y^+ = 18$ for Re350, Re600 and Re960.

IV. Conclusion

In this paper, large-eddy simulations of turbulent channel flows based on relaxation filtering are reported. In a first step, simulations of a channel flow at a fixed Reynolds number of $Re_\tau = 300$ are performed using different grids to study the influence of grid resolution on the results. A grid-convergence study is conducted by examining the mean and fluctuating velocity profiles. They do not vary significantly for mesh spacings equal to or smaller than $\Delta x^+ = 30$, $\Delta y^+_w = 1$ and $\Delta z^+ = 10$. An *a posteriori* analysis of the results indicates that the turbulent structures are well discretized by the grids, including the coarsest ones, which may appear inconsistent with the grid-convergence study. However, an *a priori* analysis based on the dissipation transfer functions associated with molecular viscosity and relaxation filtering shows that in the simulations with coarser grids, in particular when $\Delta x^+ \geq 30$, a part of the resolved turbulent scales may be affected by the relaxation filtering, which is not desirable in an LES.

In a second step, the capacity of the present LES approach to capture Reynolds number effects is considered using simulations of channel flows at $Re_\tau = 360$, 600 and 960. The mean and fluctuating streamwise velocity profiles are found to agree very well with DNS results of the literature. In particular, the emergence of a hump in the outer part of the rms velocity profiles as the Reynolds number increases is well reproduced by the LES. Concerning the streamwise velocity spectra in the buffer region, their shapes change with the Reynolds number. More precisely, it is noted that the high-wavenumber components scale in inner units, whereas the low-wavenumber components scale in outer units.

The present work demonstrates that the LES method based on relaxation filtering is an interesting tool for the study of wall-bounded flows, especially at higher Reynolds numbers which are not currently reachable by DNS.

Acknowledgments

The first author is grateful to the Direction Générale de l'Armement (DGA) and the Centre National de la Recherche Scientifique (CNRS) for financial support. This work was granted access to the HPC resources of the Institut du Développement et des Ressources en Informatique Scientifique (IDRIS) under the allocation 2012-020204 made by GENCI (Grand Equipement National de Calcul Intensif).

Références

[1]Marusic, I., McKeon, B.J., Monkewitz, P.A., Nagib, H.M., Smits, A.J. and Sreenivasan, K.R., "Wall-bounded turbulent flows at high Reynolds numbers : Recent advances and key issues," *Phys. Fluids*, Vol. 22, 2010, 065103.

[2]Kim, J., Moin, P. and Moser, R., "Turbulence statistics in fully developed channel flow at low Reynolds number," *J. Fluid Mech.*, Vol. 177, 1987, pp. 133-166.

[3]del Alamo, J.C. and Jiménez, J., "Spectra of the very large anisotropic scales in turbulent channels," *Phys. Fluids*, Vol. 15, No. 6, 2003, L41-L44.

[4]del Alamo, J.C., Jiménez, J., Zandonade, P. and Moser, R.D., "Scaling of the energy spectra of turbulent channels," *J. Fluid Mech.*, Vol. 500, 2004, pp. 135-144.

[5]Hoyas, S. and Jiménez, J., "Scaling of the velocity fluctuations in turbulent channels up to $Re_\tau = 2003$," *Phys. Fluids*, Vol. 18, 2006, 011702.

[6]Hu, Z.H., Morfey C.L. and Sandham, N.D., "Aeroacoustics of wall-bounded turbulent flows," *AIAA Journal* Vol. 40, No. 3, 2002, pp. 465-473.

[7]Hu, Z.H., Morfey C.L. and Sandham, N.D., "Wall pressure and shear stress spectra from direct simulations of channel flow," *AIAA J.* Vol. 44, No. 7, 2006, pp. 1541-1549.

[8]Moser, R.D., Kim, J. and Mansour, N., "Direct numerical simulation of turbulent channel flow up to $Re_\tau = 590$," *Phys. Fluids*, Vol. 11, No. 4, 1999, pp. 943-945.

[9]Spalart, P.R., "Direct simulation of a turbulent boundary layer up to $R_\theta = 1410$," *J. Fluid Mech.* Vol. 187, 1988, pp. 61-98.

[10]Schlatter, P., Örlü, R., Li, Q., Brethouwer, G., Fransson, J.H.M., Johansson, A.V., Alfredsson, P.H. and Henningson, D.S., "Turbulent boundary layers up to $Re_\theta = 2500$ studied through simulation and experiment," *Phys. Fluids*, Vol. 21, 2009, 051702.

[11]Simens, M.P., Jiménez, J., Hoyas, S. and Mizuno, M., "A high-resolution code for turbulent boundary layers," *J. Comput. Phys.*, Vol. 228, No. 11, 2009, pp. 4218-4231.

[12]Wu, X. and Moin, P., "Direct numerical simulation of turbulence in a nominally zero-pressure-gradient flat-plate boundary layer," *J. Fluid Mech.*, Vol. 630, 2009, pp. 5-41.

[13]Schlatter, P. and Örlü, R., "Assessment of direct numerical simulation data of turbulent boundary layers," *J. Fluid Mech.*, Vol. 659, 2010, pp. 116-126.

[14]Sagaut, P., "Large Eddy Simulation for incompressible flows," Springer, Berlin, Germany, 2006.

[15]Piomelli, U. and Balaras, E., "Wall-layer models for large-eddy simulations", *Annu. Rev. Fluid Mech.*, Vol. 34, 2002,, pp. 349-374.

[16]Chung, D. and McKeon, B.J., "Large-eddy simulation of large-scale structures in long channel flow," *J. Fluid Mech.*, Vol. 661, 2010, pp. 341-364.

[17]Viazzo, S., Dejoan, A., Schiestel, R., "Spetral features of the wall-pressure fluctuations in turbulent wall flows with and without perturbations using LES," *Int. J. Heat and Fluid Flow*, Vol. 22, 2001, pp. 39-52.

[18]Suh, J., Frankel, S.H., Mongeau, L. and Plesniak, M.W., "Compressible large eddy simulations of wall-bounded turbulent flows using a semi-implicit numerical scheme for low Mach number aeroacoustics," *J. Comput. Phys.*, Vol. 215, No. 2, 2006, pp. 526-551.

[19]Gloerfelt, X. and Berland, J., "Direct computation of turbulent boundary layer noise" *15th AIAA/CEAS AeroAcoustics Conference*, 11-13 May, Miami, Florida, USA, AIAA Paper 2009-3401.

[20]Schlatter, P., Li, Q., Brethouwer, G., Johansson, A.V., and Henningson, D.S., "Simulations of spatially evolving turbulent boundary layers up to $Re_{\tilde{T}} = 4300$," *Int. J. Heat and Fluid Flow*, Vol. 31, 2010, pp. 251-261.

[21]Schlatter, P. and Örlü, R., "Turbulent boundary layers at moderate Reynolds numbers : inflow length and tripping effects," *J. Fluid Mech.*, Vol. 710, 2012, pp. 5-34.

[22]Rasam, A., Brethouwer, G., Schlatter, P., Li, Q. and Johansson, A.V., "Effects of modelling, resolution and anisotropy of subgrid-scales on large eddy simulations of channel flow," *J. Turb.*, Vol. 12, No. 10, 2010, pp. 1-20.

[23]Vuorinen, V., Larmi, M., Schlatter, P., Fuchs, L. and Boersma, B.J., "A Low-Dissipative, Scale-Selective Discretization Scheme for the Navier-Stokes Equations," *Comp. & Fluids*, Vol. 70, 2011, pp. 195-205.

[24]Bogey, C., de Cacqueray, N. and Bailly, C., "A shock-capturing methodology based on adaptative spatial filtering for high-order non-linear computations," *J. Comput. Phys.*, Vol. 228, No. 5, 2009, pp. 1447-1465.

[25]Bogey, C. and Bailly, C., "Turbulence and energy budget in a self-preserving round jet : direct evaluation using large eddy simulation", *J. Fluid Mech.*, Vol. 627, 2009, pp. 129-160.

[26]Bogey, C. and Bailly, C., "Large Eddy Simulations of transitional round jets : influence of the Reynolds number on flow development and energy dissipation," *Phys. Fluids*, Vol. 18, No. 6, 2006, 065101.

[27]Bogey, C. and Bailly, C., "Large eddy simulations of round free jets using explicit filtering with/without dynamic Smagorinsky model," *Int. J. Heat and Fluid Flow*, Vol. 27, 2006, pp. 603.

[28]Bogey, C., Marsden, O., and Bailly, C., "Large-Eddy Simulation of the flow and acoustic fields of a Reynolds number 10^5 subsonic jet with tripped exit boundary layers," *Phys. Fluids*, Vol. 23, 2011, 035104.

[29]Bogey, C., Marsden, O., and Bailly, C., "Effects of moderate Reynolds numbers on subsonic round jets with highly

disturbed nozzle-exit boundary layers," *Phys. Fluids*, Vol. 24, 2012, 105107.
[30]Marden, O., Bogey, C., and Bailly, C., "Direct noise computation of the turbulent flow around a zero-incidence airfoil," *AIAA J.* Vol. 46, No. 4, 2008, pp. 874-883.
[31]Bogey, C. and Bailly, C., "A family of low dispersive and low dissipative explicit schemes for flow and noise computations," *J. Comput. Phys.*, Vol. 194, No. 1, 2004, pp. 194-214.
[32]Berland, J., Bogey, C. and Bailly, C., "Low-dissipation and low-dispersion 4th-order Runge-Kutta algorithm," *Comp. & Fluids*, Vol. 35, 2006, pp. 1459-1463.
[33]Kremer, F., Bogey, C., and Bailly, C., "Development of semi-implicit Runge-Kutta schemes and application to a turbulent channel flow," *18th AIAA/CEAS Aeroacoustics Conference*, 4-6 June, Colorado Springs, Colorado, USA, AIAA Paper 2012-2066.
[34]Robinson, S.K., "A review of vortex structures and associated coherent motions in turbulent boundary layers", *Annu. Rev. Fluid Mech.*, Vol. 23, 1991, pp.601-39.
[35]Coles, D., "The law of the wake in the turbulent boundary layer," *J. Fluid Mech.* Vol. 1, 1956, pp. 191-226.
[36]Nagib, H.M., and Chauhan, K.A., "Variations of von Krmn coefficient in canonical flows", *Phys. Fluids*, Vol. 20, 2008, 101518.
[37]Kline, S.J., Reynolds, W.C., Schraub, F.A. and Runstadler, P.W., "The structure of turbulent boundary layers," *J. Fluid Mech.* Vol. 30, 1967, pp. 741-773.
[38]Tomkins, C.D. and Adrian, R.J., "Energetic spanwise modes in the logarithmic layer of a turbulent boundary layer," *J. Fluid Mech.*, Vol. 545, 2005, pp. 141-162.